Journal of Nuclear Materials 396 (2010) 65–70

Contents lists available at ScienceDirect

Journal of Nuclear Materials

journal homepage: www.elsevier.com/locate/jnucmat

Crystal structure, corrosion kinetics of new zirconium alloys and residual stress analysis of oxide films

H.X. Zhang [a,b,c], D. Fruchart [b,*], E.K. Hlil [b], L. Ortega [b], Z.K. Li [c], J.J. Zhang [c], J. Sun [a], L. Zhou [c]

[a] Xi'an Jiaotong University, Xi'an 710049, China
[b] Institut Néel, CNRS, BP 166, 38042 Grenoble, Cedex 9, France
[c] Northwest Institute for Nonferrous Metal Research, Xi'an 710016, China

ARTICLE INFO

Article history:
Received 27 January 2008
Accepted 20 October 2009

ABSTRACT

Corrosion kinetics of NZ2 alloy were investigated after autoclave treatments in 360 °C/18.6 MPa lithiated water and 400 °C/10.3 MPa steam. The crystal structure and the residual stress of oxide films of NZ2 alloys after corroded in both conditions were investigated by XRD method. The kinetics analysis indicates that the resistance of NZ2 alloy treated in 360 °C lithiated water is higher than that treated in 400 °C steam. The crystal structure analysis shows that the content of tetragonal t-ZrO_2 in the oxide films decreases smoothly and the content of monoclinic m-ZrO_2 increases with the duration of corrosion time, independent of the kinetics transition. Stress measurements show that high compressive stresses were developed in the oxide layers. Furthermore, the transitions of kinetics can be associated with the sudden decrease of macroscopic compressive stresses in the oxide films. The higher t-ZrO_2 content is, the higher compressive stress in the oxide film is, the lower is the corrosion rate. Therefore it is considered that t-ZrO_2 is mainly stabilized by the macroscopic compressive stresses in the oxide films. In addition, local stresses in the oxide films, grain size and the oxygen vacancies play an important role in the t-ZrO_2 stabilization.

1. Introduction

Zirconium alloys, identified as zircaloys, are the major structure materials used in water-cooled nuclear power reactors such as fuel claddings, fuel channels, etc. Interests for zircaloys result from the low neutron absorption cross section of zirconium, the high mechanical strength and the good corrosion resistance. The oxide film formed on the pressurized tube surface forms a rather good protective barrier against further oxidation which extends the tubes life. It is obvious that further significant improvement in corrosion resistance requires a deep corrosion processes understanding. Therefore, a fundamental understanding of the crystalline and physical properties of the oxide layer during the corrosion process is needed.

Numerous reports [1–5] points to idea that the oxide comprises a tetragonal ZrO_2 (t-ZrO_2) phase and a more stable monoclinic ZrO_2 (m-ZrO_2) phase. The former phase develops under local conditions when oxide is formed, such as stresses, smallness of grain size and presence of dissolved alloying elements in the metal. The phase formation and their transformation in the oxide films result from rather complicated processes occurring throughout corrosion duration. Most of related studies emphasize the close relationship between the amount of t-ZrO_2 and the corrosion resistance. In fact, some works specifically confirm that high compressive stresses, in relation with a high Pilling–Bedworth ratio of 1.56 for the couple ZrO_2/Zr, are developed in the oxide film formed at surface of zircaloys. These compressive stresses are found closely related to both the corrosion kinetics and the microstructure of the grown oxide layers so that they influence directly the corrosion mechanisms [6–13].

The aim of the present work is to provide additional insights in the relationship between the structure, the residual stress state of the oxide layers formed on selected zirconium alloys and the related corrosion behavior. For this study, pieces of a NZ2 alloy, which formula is displayed in Table 1, were corroded in 360 °C/18.6 MPa lithiated water and 400 °C/10.3 MPa steam conditions. Crystal structure and the compressive stresses of the resulting oxide films were characterized by X-Ray Diffraction (XRD).

2. Experimental

NZ2 alloy plates were submitted to preliminary annealing processes of 650 °C for 2 h, 590 °C for 3 h and 590 °C for 3 h,

* Corresponding author.
E-mail address: daniel.fruchart@grenoble.cnrs.fr (D. Fruchart).

0022-3115/$ - see front matter © 2009 Elsevier B.V. All rights reserved.
doi:10.1016/j.jnucmat.2009.10.055

Table 1
Chemical composition of the NZ2 alloy used in the investigation (wt.%).

Sn	Nb	Fe	Cr	O	Zr
1.0	0.3	0.3	0.1	0.08–0.14	Balance

Table 2
Weight gain, exposure time, thickness of the oxide films of NZ2 alloy and the d vs. ψ plot slopes.

Corrosion conditions	Exposure duration (days)	Weight gain (mg/dm^2)	Oxide film thickness (μm)	The *d* vs. *ψ* plot slope
360 °C lithiated water				
	3	12.88	0.9	
	14	18.50	1.2	−0.0132
	28	22.85	1.5	−0.0188
	42	25.92	1.7	−0.0169
	70	30.20	2.0	−0.0228
	98	34.53	2.3	−0.0149
	126	37.85	2.5	−0.0148
	154	58.56	1.8	−0.0111
	182	68.08	4.5	
	210	72.90	4.9	−0.0101
	238	77.28	5.2	−0.0117
	294	104.15	6.9	
400 °C steam				
	3	17.00	1.1	−0.0119
	14	26.14	1.7	−0.0152
	28	32.42	2.2	−0.0174
	42	37.47	2.5	−0.0130
	70	51.63	3.4	
	98	62.32	4.2	−0.0086
	126	72.97	4.9	
	154	82.47	5.5	−0.0098
	238	116.14	7.7	−0.0098
	266	119.65	8.0	−0.0093

respectively. Long-term corrosion tests of plates were performed in static autoclave conditions either at 360 °C under 18.6 MPa in lithiated water or at 400 °C under 10.3 MPa pressure steam.

For the present study, corrosion of various NZ2 alloy specimens were tested simultaneously in single autoclaves which tests were periodically interrupted to measure the weight gain. Table 2 displays the exposure time, weight gain and the oxide film thickness of samples chosen for XRD analysis after the oxidation tests. Oxide layers thickness was estimated from the weight gain using the relationship 1 μm = 15 mg/dm^2. For a complete analysis, two typical parameters were considered; first the *d*-spacing of (*hkl*) diffraction planes and then *ψ* the angle between the normal of the sample surface and the [*hkl*] diffraction vectors. The slopes of the *d* vs. *ψ* plots of oxide films, measured for stress analysis, are reported in Table 2. Grazing incidence XRD experiments were performed using a PW3830 X-ray power supply with $Fe_{K\alpha}$ radiation in order to characterize the oxidized surface structure. The relationship between the grazing incident angle and the probed thickness is shown in Fig. 1. Classical X-ray diffractometry measurements were performed as well using a PW3830 X-ray power supply with $Cu_{K\alpha}$ radiation in order to test the crystal structure, the average phase content and the residual stresses of the total oxide films.

3. Results

3.1. Corrosion kinetics

Fig. 2 shows the corrosion kinetics traces of NZ2 alloys after being treated in 360 °C lithiated water and in 400 °C steam. The corrosion rate of NZ2 alloy in 360 °C lithiated water appears lower than those samples submitted to 400 °C steam. The oxidation

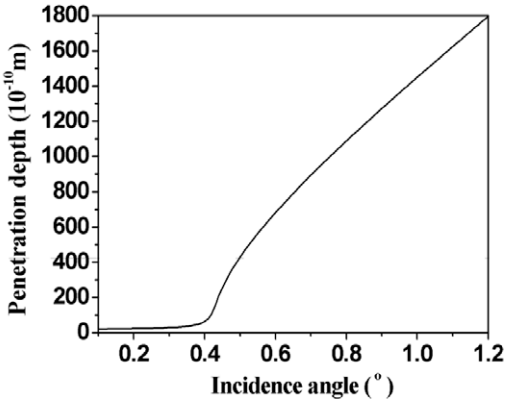

Fig. 1. Probed thickness of oxide film vs. incidence angles.

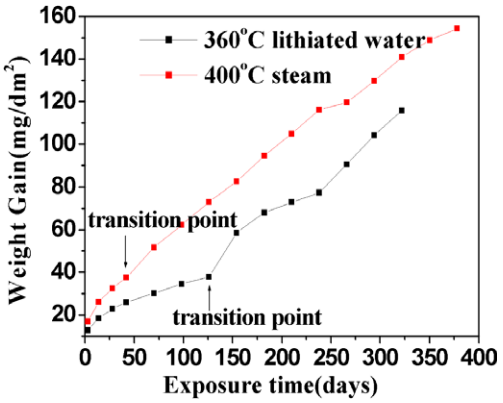

Fig. 2. Corrosion kinetics of NZ2 alloy in 360 °C lithiated water and 400 °C steam.

kinetic traces initially follow either a parabolic or a cubic type progression before the oxide transformation has occurred. Typical transformation duration was for 126 days and 42 days in both experimental conditions, respectively. The reason for such transformation has not yet been fully established; but it was expected related to the accumulation of strains in the oxide films and the subsequent development of porosities even large-scale cracks [1,14,15].

3.2. t-ZrO_2 content and crystal structure in the oxide films

Figs. 3 and 4 display grazing incidence XRD patterns of oxide film surface for NZ2 alloy exposed to 360 °C lithiated water and 400 °C steam during 3 days, respectively. According to Fig. 1, the probed thicknesses corresponding to 0.2, 0.3, 0.5 and 1.0° grazing incidence angles, are 0.002, 0.003, 0.043 and 0.145 μm, respectively. It is clear that the intensity of the (1 0 1) Bragg peak for t-ZrO_2 increases from the outer to the inner part of the oxide films. Besides, the t-ZrO_2 content in the oxide layer is found larger when the alloy was processed in lithiated water at 360 °C than in steam at 400 °C, for the same duration of 3 days.

Fig. 5 shows the grazing incidence XRD patterns of oxide film surface of NZ2 alloy exposed to 360 °C lithiated water for 3 days (trace A) and 182 days (trace B), respectively. The grazing incidence angle was 1.0° and the probed thickness of oxide film was 0.145 μm. In trace A, the (1 0 1) Bragg peak intensity of t-ZrO_2 was found larger than the (1 1 1) one of m-ZrO_2. However, the results are found opposite in trace B. This means that the t-ZrO_2 content in the oxide layer has decreased whereas the content of m-ZrO_2 has increased vs. corrosion process duration, i.e. the

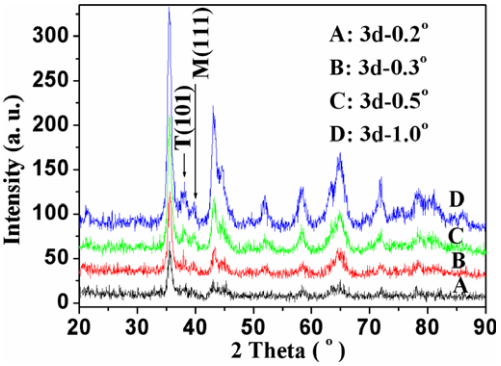

Fig. 3. Grazing incidence XRD patterns of the oxide film surface of NZ2 alloy exposed to 360 °C lithiated water for 3 days (d).

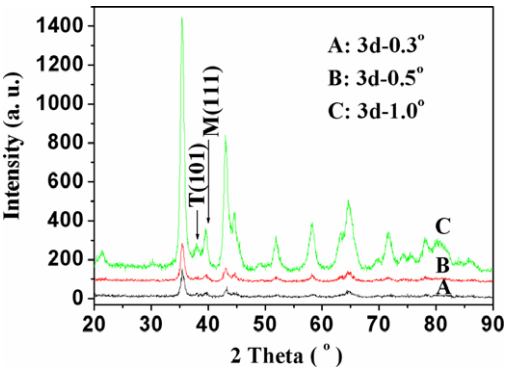

Fig. 4. Grazing-incidence XRD patterns of the oxide film surface for a NZ2 alloy exposed to 400 °C steam for 3 days (d).

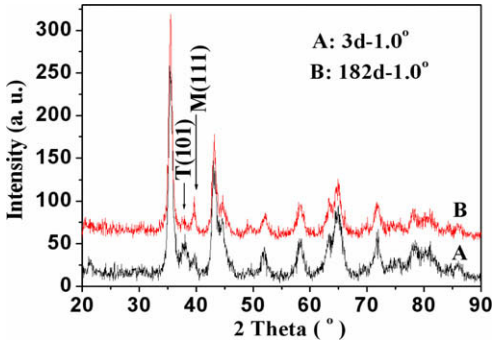

Fig. 5. Grazing-incidence XRD patterns of the oxide film surface for a NZ2 alloy exposed to 360 °C lithiated water for different times.

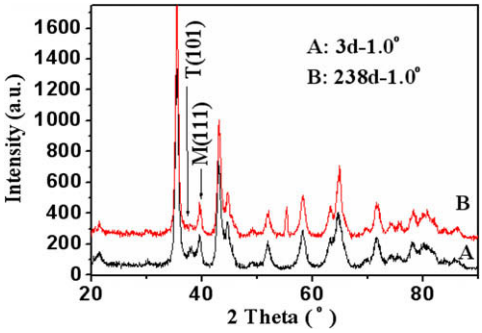

Fig. 6. Grazing-incidence XRD patterns of the oxide film surface for a NZ2 alloy exposed to 400 °C steam for different times.

t-ZrO_2 transforms to m-ZrO_2. Fig. 6 shows the grazing incidence XRD pattern of oxide surface for NZ2 alloy exposed to 400 °C steam for 3 days and 238 days, respectively. The results are consistent with those of Fig. 5, namely, t-ZrO_2 transforms to m-ZrO_2 upon prolongation of corrosion duration.

From the reported grazing incidence XRD analyses, the oxide layer outer side of NZ2 alloy was found to consist mostly of m-ZrO_2, including a small amount of t-ZrO_2. As a result, the higher is the t-ZrO_2 content the better is the corrosion resistance.

Fig. 7 shows the normal XRD patterns of the oxide film of NZ2 alloy exposed to 360 °C lithiated water for different durations. It is worth to note that the m-(0 0 2) Bragg peak intensity increases and that of t-(0 0 2) one decreases upon the corrosion process duration. In agreement with the results of grazing incidence angle XRD, t-ZrO_2 transforms to m-ZrO_2. Fig. 8 shows the same result during the oxidation of NZ2 at 400 °C in steam. The total integrated intensities $I(hkl)$ of the m-(-1 1 1), m-(1 1 1) and t-(1 0 1) were used to determine the t-ZrO_2 volume fraction f_T with respect to the total volume of zirconia using the Garvie–Nicholson formula [16]:

$$f_T = \frac{I_T(101)}{I_T(101) + I_M(111) + I_M(-111)} \quad (1)$$

The result of calculation, as shown in Fig. 9, validates the above conclusions. However, the use of such formula is likely biased because of the strong texture effect existing in the oxide films. A better determination of the relative proportion of the t-ZrO_2 and m-ZrO_2 phases needs additional experiment and analyses, e.g. precise texture determination. Here, analysis is only a guide to appreciate the main impacts of the corrosion duration on the oxide layers.

Fig. 9 shows the relationship between the growth of t-ZrO_2 in oxide films obtained at 400 °C and at 360 °C in lithiated water. In this Figure, the thickness variation of the t-ZrO_2 layer is presented in relative scale, reference to the total amount of formed oxide. Typically about 1 μm total oxide layer was achieved for ~150 day exposure in 400 °C steam condition. Fig. 9 shows that the relative value of t-ZrO_2 generated in lithiated water remains more than twice that is observed under steam conditions. Moreover, the difference of temperature (from 360 °C to 400 °C) can be considered as an additional parameter favoring the formation of less relative proportion of t-ZrO_2 layers during the second experiment. Nevertheless, the experimental variation of the t-ZrO_2 relative proportion in both conditions (360 °C lithiated water, 400 °C steam) fit fairly well to a $A\,e^{-\alpha x}$ type law. Interestingly, the α exponent gets the unique value of -33×10^{-5}: the rate of t-ZrO_2 transformation is found the same in both experiments. From the normal XRD patterns, it appears that the relative content of t-ZrO_2 within the oxide film diminishes reference to the amount of m-ZrO_2 which increases with the corrosion process duration. The tetragonal t-ZrO_2 transforms to m-ZrO_2 continuously and smoothly in the duration range studied; but no abrupt change was detected in terms of transition kinetics.

3.3. Stress determination in the oxide layer

The mean residual stress determination by using XRD method implies the lattice parameters as local strain gauges. Microstrains are given by the relation:

$$\varepsilon = \left(\frac{d - d_0}{d_0}\right)_{hkl} = -\frac{1}{2}\cot g\theta_0 * (2\theta - 2\theta_0) \quad (2)$$

where, d_0 is the stress free interatomic distance of the (hkl) reflecting planes, θ_0 is the stress free Bragg peak position. The stresses of lattice were measured from diffraction and the elastic stresses were determined by micromechanical analysis. In a standard procedure,

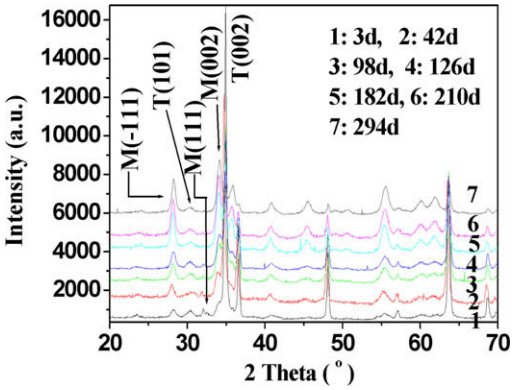

Fig. 7. Normal XRD patterns of oxide film of NZ2 alloy exposed to 360 °C lithiated water for different durations.

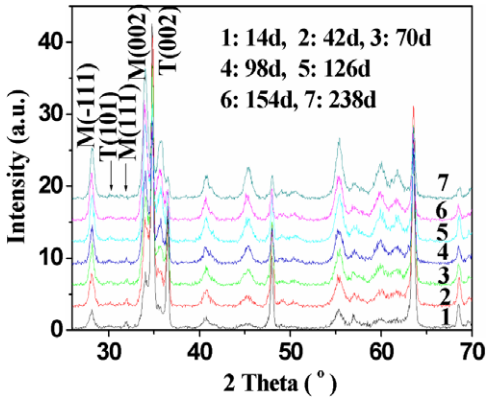

Fig. 8. Normal XRD patterns of oxide film of NZ2 alloy exposed to 400 °C steam for different durations.

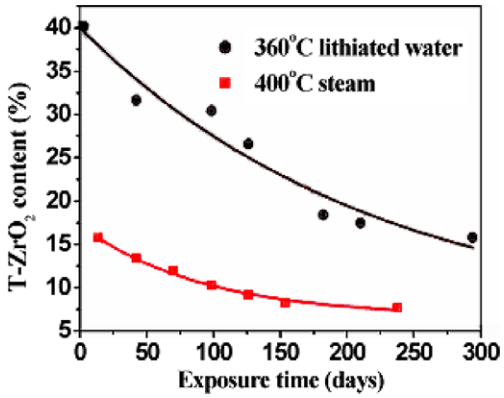

Fig. 9. Relationship of corrosion duration and the t-ZrO_2 content in oxide film of NZ2 alloy.

the material is assumed to be homogeneous and isotropic. Lattice stresses were considered homogeneously dispatched in the probed diffracting volume [17].

The interplanar distances vary vs. ψ, e.g. if macroscopic strains are developed in the material. The diffraction peak shift can be estimated from the following formula:

$$2\theta = 2\theta_0 - \left(\frac{1}{2}S_2\right)\frac{360}{\pi}\tan\theta_0[\sigma_{11}\sin^2\psi + \sigma_{13}\sin(2\psi)] - (S_1) \times \frac{360}{\pi}\tan\theta_0[\sigma_{11}+\sigma_{22}] \quad (3)$$

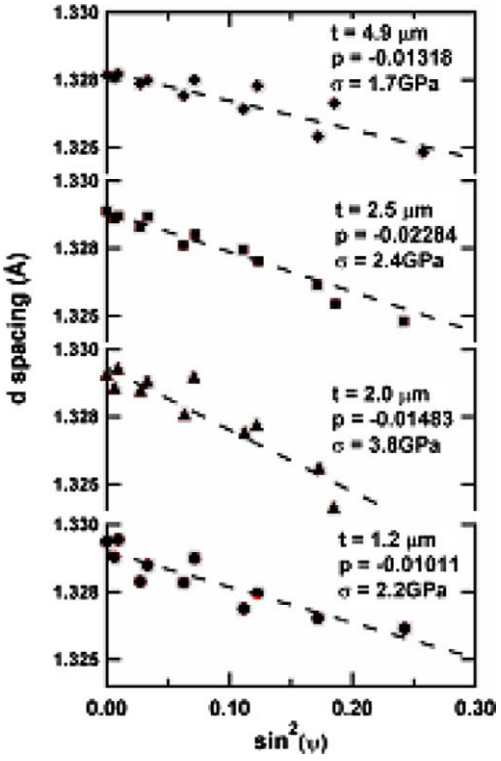

Fig. 10. The $d = f(\sin^2\psi)$ plots of samples corroded in 360 °C lithiated water for 14d, 70d, 126d and 210d.

where, the σ_{ij} are the components of stress intensity tensor, $\frac{1}{2}S_2$ and S_1 represent the elastic constants defined for isotropic materials by:

$$\frac{1}{2}S_2 = \frac{1+\nu}{E} \quad \text{and} \quad S_1 = \frac{-\nu}{E} \quad (4)$$

where, ν is the Poisson's coefficient. For the oxide film formed at NZ2 surfaces, stresses have a bi-dimensional character ($\sigma_{11} = \sigma_{22}$, $\sigma_{13} = 0$). So, one can estimate the distance d from relations (III) and (IV) leading to:

$$d = \left(\frac{1+\nu}{E}\right)d_0\sigma_{11}\sin^2\psi - \frac{2\nu}{E}\sigma_{11}d_0 + d_0 \quad (5)$$

Then σ_{11} is deduced from the slope p of the d vs. $\sin^2\psi$ linear fit [18]:

$$p = \left(\frac{1+\nu}{E}\right)d_0\sigma_{11}, (E = 281\ GPa \text{ and } \nu = 0.29)\ [18] \quad (6)$$

As usually reported, here the residual stresses in the oxide films of samples oxidized in 360 °C lithiated water and in 400 °C steam were determined from (VI) for the $(\bar{1}04)_m$ planes of m-ZrO_2 (for angular position $2\theta_0 = 71.226^0$ at $\lambda = Cu_{K\alpha}$) [19,20]. The d vs. $f(\sin^2\psi)$ plots were analyzed and some significant results are displayed in Figs. 10 and 11, in which the corresponding thickness, slope and stress levels are indicated. The slopes of the d vs. ψ plots, obtained from all the samples after treatments in both conditions, are displayed in Table 2. The slope changes vs. the corrosion duration as well as vs. the thickness of oxide film, meaning that the residual stress changes consequently. The relationship established between the oxide film thickness and the residual stress values exactly confirm what it was earlier determined in reference 9 as recalled here in Fig. 12. Negative values of the stress levels indicate compressive residual effects in the oxide layers grown in both conditions (liquid and steam). The compressive stress levels seem to increase with thickness of the film, reaching a maximum values when the oxide thickness is about 2.0 µm for 360 °C lithiated water

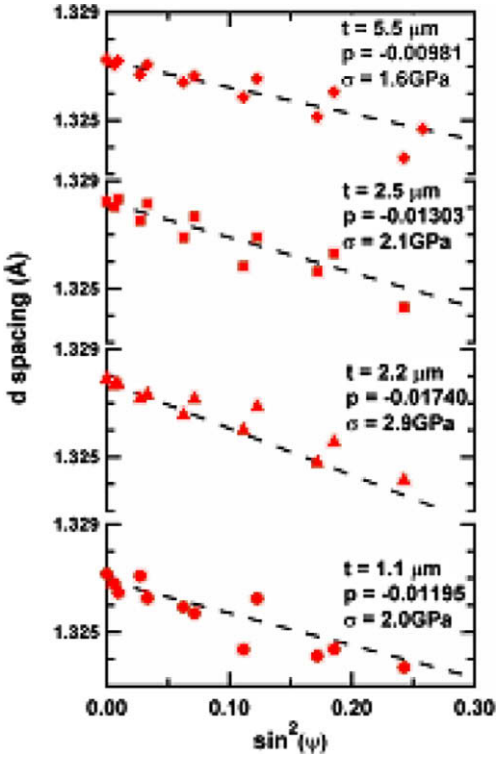

Fig. 11. The $d = f(\sin^2\psi)$ plots of samples corroded in 400 °C steam for 3d, 28d, 42d, 154d and 238d.

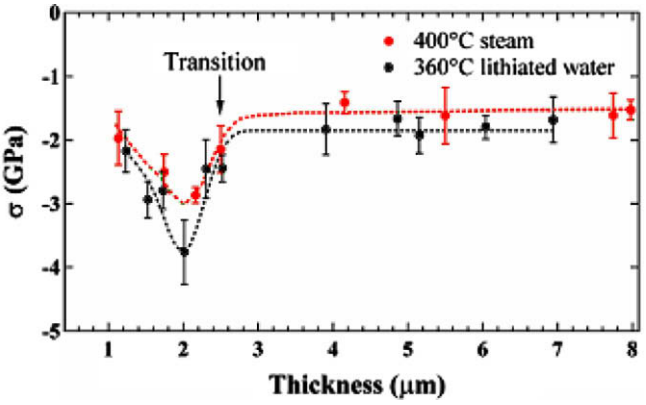

Fig. 12. Relationship of the oxide film thickness and compressive stresses in oxide film of NZ2 alloy corroded at 360 °C lithiated water and at 400 °C in steam.

and 2.2 μm for 400 °C steam treatments, respectively. Afterwards, they decrease significantly and the stress levels of post-transition samples become steady. Comparing the stress values of the samples as corroded in both media, the average compressive stress levels after treatment in 360 °C lithiated water are higher than those after treatment in 400 °C steam. The mean stress value in oxide films of NZ2 is 1.5–3.8 GPa, in fair agreement with what was reported earlier [21,22]. The corrosion transition appears associated with a sudden stress level release. In fact, the oxide films formed on NZ2 alloy are strongly textured. The level of stress measured on the $(\bar{1}04)$ planes of m-ZrO_2 is only an estimate of the average stress tensor components developed in the layer. However, the levels of stress here estimated can be used quantitatively to correlate stress state, the phase fractions and the corrosion kinetics.

4. Discussion

The main points to be discussed are the transformations in the oxide film, the relationship between the phases, the stress changes and the oxidation kinetic rates.

It is clear that the average t-ZrO_2 content decreases smoothly but continuously as the oxidation proceeds, independent of the kinetic transitions in both oxidization media. Obviously, there is no sharp or sudden evolution throughout the bulk of the oxide film. In terms of corrosion kinetics as promoted in both oxidization media, high t-ZrO_2 contents are expected improving the corrosion resistance since this phase remains compact.

The present experiments suggest that the compressive stress level increases when begins oxidation. In the formed oxide films, compressive strains exceed a critical value so that a stress relaxation occurs when the oxide film thickness reaches a given value of about 2 μm. The relaxation process, corresponding to the kinetic transition, induces cracks and porosities in the oxide layers, thus degrading the protective properties of the oxide and accelerating further attacks. Then, the compressive stress level remains very low within samples in post-transition state at about 1.9 GPa for samples treated in 360 °C lithiated water and at 1.6 GPa for samples treated in 400 °C steam. Also to highest compressive stress levels developed in 360 °C lithiated water corresponds a better corrosion resistance of samples.

With respect to the relation between the t-ZrO_2 content and compressive stress value, it is guessed that the higher t-ZrO_2 content corresponds to the highest compressive stress as a whole. During the corrosion process, the zirconia layer is less dense than the metal substrate, the forced expansion induces high compressive stresses in the oxide in relation with the high Pilling–Bedworth ratio of the Zr/ZrO_2 system [13,22,23]. Hence, the compressive stresses developed in the oxide play an important role for the further stability of t-ZrO_2 which was said to form compact oxide scale where the compressive stresses are higher [24]. However, in the present work, it is shown that there is no full consistency between the rate of t-ZrO_2 content and the compressive stress value. Nevertheless, one should remind that the t-ZrO_2 compacts are not uniformly distributed and there is a higher content near the metal/oxide interface as shown from grazing XRD experiments. Then, local sharp decrease at the metal/oxide interface for thick oxide layers is not excluded and inevitably there are areas submitted to high local stress concentration. Besides, the stresses measured here are of macroscopic compressive stress type. More probably it is not enough to consider only macroscopic compressive stresses in order to justify the experiment results. So, in agreement with Ref. [25], local stresses may play an important role in the stabilization of t-ZrO_2.

5. Conclusion

NZ2 alloy samples were oxidized either in 360 °C lithiated water or in 400 °C steam. The macroscopic stresses and the t-ZrO_2 content in the oxide films were analyzed by XRD. It was established that:

(1) The major part of NZ2 oxide in films is of m-ZrO_2 type, with a minor part of t-ZrO_2. With corrosion time prolongation, the t-ZrO_2 content in the overall oxide film decreases smoothly and the m-ZrO_2 content increases correspondingly, independent of the kinetic transitions: the t-ZrO_2 transforms to m-ZrO_2.

(2) High compressive strains are pointed out in the oxide layers. The corrosion transition is associated with a sudden release of the macroscopic compressive stresses in the oxide films.

(3) The samples treated in 360 °C lithiated water present lower corrosion kinetics than that treated in 400 °C steam, but highest t-ZrO_2 content and highest compressive stresses. The t-ZrO_2 is therefore mainly stabilized by the macroscopic compressive stresses. In addition, as the local stresses in the oxide films, the grain size and the oxygen vacancies play a significant role in the t-ZrO_2 stabilization.

References

[1] J. Godlewski, J.P. Gros, M. Lambertin, J.F. Wadier, H. Weidinger, in: 9th International Symposium on Zr in the Nuclear Industry, ASTM STP 1132, Kobe, Japan, 1991, p. 416.
[2] K. Takeda, H. Anada, in: 12th International Symposium on Zr in the Nuclear Industry, ASTM STP 1354, Toronto, Canada, 2000, p. 592.
[3] J.H. Baek, Y.H. Jeong, I.S. Kim, J. Nucl. Mater. 280 (2000) 235.
[4] A. Yilmazbayhan, A.T. Motta, R.J. Comstock, G.P. Sabol, B. Lai, Z.H. Cai, J. Nucl. Mater. 324 (2004) 6.
[5] J. Krýsa, J. Maixner, P. Matějka, V. Vrtílková, Mater. Chem. Phys. 63 (2000) 1.
[6] H. Anada, K. Takeda, in: 11th International Symposium on Zr in the Nuclear Industry, ASTM STP, 1996, p. 35.
[7] T. Arima, K. Miyata, Y. Inagaki, K. Idemitsu, Corros. Sci. 47 (2005) 435.
[8] A.P. Zhiyaev, J.A. Szpunar, J. Nucl. Mater. 264 (1999) 327.
[9] M.G. Glavicic, Ph.D. Thesis, McGill University, Canada, 1998.
[10] N. Pétigny, P. Barberis, C. Lemaignan, Ch. Valot, M. Lallemant, J. Nucl. Mater. 280 (2000) 318.
[11] M. Oskarsson, E. Ahlberg, U. Andersson, K. Pettersson, J. Nucl. Mater. 297 (2001) 77.
[12] J. Godlewski, Ph.D. Université de Compiègne: Oxydation d'alliages de zirconium en vapeur d'eau: influence de la zircone tétragonale sur le mécanisme de croissance de l'oxyde, 1990.
[13] F. Garzarolli, H. Seidel, R. Tricot, J.P. Gros, ASTM STP 1132, 1991, p. 395.
[14] H.G. Weidinger, H. Ruhmann, G. Cheliotis, M. Maguire, T.-L. Yau, in: 9th International Symposium on Zr in the Nuclear Industry, ASTM STP 1132, Kobe, Japan, 1991, p. 499.
[15] A.T. Motta, A. Yilmazbayhan, R.J. Comstock, J.M. Partezana, G.P. Sabol, B. Lai, Z. Cai, J. ASTM Int. 2 (2005).
[16] R.C. Garvie, P.S. Nicholson, J. Am. Ceram. Soc. 55 (1972) 303.
[17] O.V. Hauk, Adv. X-ray Anal. 39 (1997) 181.
[18] H.J. Beie, A. Mitwalsky, F. Garzarolli, H. Ruhmann, H.J. Sell, ASTM STP 1245, 1994, p. 615.
[19] J. Godlewski, J.P. Gros, M. Lambertin, J.F. Wadier, H. Weidinger, ASTM-STP-1132, 1991, p. 416.
[20] J.L. Béchade, P. Goudeau, M. Gailhanou, P. Yvon, High Temp. Mater. Processes 2 (1998) 359.
[21] L. Gosmain, C. Valot, D. Ciosmak, O. Sicardy, Solid State Ionics 141–142 (2001) 633.
[22] C. Roy, B. Burgess, Oxid. Met. 2 (1970) 235.
[23] J. Godlewski, P. Bouvier, G. Lucazeau, L. Fayette, ASTM STP 1354, 2000, p. 877.
[24] N. Petigny-Putigny, Ph.D. Université de Bourgogne: Comparaison de l'oxydation de deux alliages de zirconium par diffraction des rayons X in-situ et ex-situ: texture, phase, contrainte, Dijon, 1998.
[25] W. Qin, C. Nam, H.L. Li, J.A. Szpunar, J. Alloys Compd. 437 (2006) 280.